BCKDK regulates the TCA cycle through PDC to ensure embryonic development in the absence of PDK family

Lia Heinemann-Yerushalmi,[*1] Lital Bentovim,[*1] Neta Felsenthal,[1] Nofar Michaeli,[1] Sharon Krief,[1] Rebecca Haffner-Krausz,[2] Shifra Ben-Dor,[3] Maxim Itkin,[4] Sergey Malitsky,[4] Alon Silberman,[5] Ayelet Erez[5] and Elazar Zelzer[1]

[1] Department of Molecular Genetics, Weizmann Institute of Science, 234 Herzl St, Rehovot 7610001, Israel

[2] Department of Veterinary Resources, Weizmann Institute of Science, 234 Herzl St, Rehovot 7610001, Israel

[3] Bioinformatics and Biological Computing Unit, Biological Services, Weizmann Institute of Science, Rehovot, 76100, Israel

[4] Department of Life Sciences Core Facilities, Weizmann Institute of Science, Rehovot, Israel

[5] Department of Biological regulation, Weizmann Institute of Science, Rehovot, Israel

*These authors equally contributed to this paper.

Correspondence:

Elazar Zelzer eli.zelzer@weizmann.ac.il

Abstract

Pyruvate dehydrogenase kinase family of enzymes (PDK1-4) are central negative regulators of the TCA cycle by phosphorylating the rate-limiting multi-enzyme pyruvate dehydrogenase complex (PDC). Here, we show that the PDK family is dispensable for murine embryonic development and that BCKDK serves as a compensatory mechanism for PDKs by inactivating PDC.

To study the role of *Pdk* family in vivo, we knocked out all four genes one by one. Surprisingly, *Pdk* total KO mouse embryos developed and were born in the expected ratio. Postnatally, these mice died by day four due to hypoglycemia or ketoacidosis, as confirmed by deep metabolic profiling.

Looking for the mechanism that enables development in the absence of *Pdk*'s, we found that PDC site 2 (S300) was phosphorylated in these embryos, suggesting that another kinase compensates for the PDK family. Bioinformatic analysis predicted brunch chain ketoacid dehydrogenase kinase (*Bckdk)*, a key regulator in the catabolism of branched chain amino acids (BCAA), as a candidate. Knockout of both *Bckdk* and the entire *Pdk* family led to loss of PDC phosphorylation on S300 and early embryonic lethality which firmly establish the role of BCKDK in the regulation of PDC. Altogether, this work demonstrates a redundancy for the PDK family during development and identifies BCKDK regulation of PDC as a backup mechanism that allows embryonic development. More broadly, BCKDK regulation of PDC reveals a new regulatory crosstalk hardwiring BCAA and glucose catabolic pathways, which feed the TCA cycle.

Introduction

The pyruvate dehydrogenase complex (PDC) plays a major role as the gatekeeper that links glycolysis to the TCA cycle, maintaining metabolic balance and energy production through the rate-limiting and physiologically irreversible oxidative decarboxylation of pyruvate [1]. Due to its importance, PDC regulation has been extensively studied since its discovery in the late 1960's [2]. The regulatory mechanism was shown to involve reversible phosphorylation by intrinsic regulatory enzymes, a family of pyruvate dehydrogenase kinases (PDK) 1-4 [3]. These isoenzymes phosphorylate and inactivate PDC on three serine residues of its catalytic E1α subunit (PDHA1), namely S293 (site 1), S300 (site 2), and S232 (site 3). Studies of site specificity showed that all four PDKs phosphorylate site 1 and site 2, whereas site 3 is phosphorylated only by PDK1. Yet, phosphorylation of any of the three serine residues leads to complete inactivation of PDC activity [4].

PDK activity blocks the flux of pyruvate into the TCA cycle, which results in a metabolic shift to glycolysis for energy production. PDC activity is regulated by *Pdk* family in a short and long-term manner[5]. In the short term, several allosteric regulators can activate PDK according to the levels of end products, namely increased acetyl-CoA/coenzyme A ratio and reduced and oxidized nicotinamide adenine dinucleotide ($NADH/NAD^+$) ratio[6]. In the long term, the amount of PDK protein is determined by different physiological conditions and in a tissue-specific manner [7–10]. This involves transcriptional and translational regulation via hormonal regulators, such as estrogen receptor and glucocorticoid receptor[11], and transcription factors such as oxygen sensor hypoxia inducible factor 1 subunit alpha (HIF1α) [12–18]. HIF1α regulation of *Pdk* was shown to occur in cancer cells, which prefer to maintain aerobic metabolism even in the presence of oxygen, a phenomenon known as the Warburg effect. Here, the increase in glycolysis supplies intermediates for branching

pathways that synthesize the macromolecules necessary for cell proliferation[19]. Based on these studies, *Pdk* family and specifically PDK1 became a specific target for anti-cancer drug development [5,20]. In addition to its role in cancer, the HIF1-PDK axis is also vital for mammalian embryonic development[21–23]. For example, during endochondral bone formation, HIF1α is required for various processes in the hypoxic growth plate [24–28], one of which is to directly regulate the expression of *Pdk1* [29].

Extensive studies on the involvement of the *Pdk* family in metabolic regulation have provided some indications for functional redundancy among its members. Cell culture experiments showed redundancy between PDK1 and PDK2 [30], whereas loss-of-function studies in mice lacking *Pdk2*, *Pdk4* or even both revealed no major effect [30–32]. Nevertheless, the question of the necessity of the four PDK isoenzymes and the functional redundancy among them has yet to be addressed by a direct genetic approach.

In this study, we investigated the requirement of Pdk's for embryonic development using the hypoxic growth plate as a model. Strikingly, mouse strains of double, triple and eventually quadruple KO, i.e. mice lacking all four *Pdk* genes, displayed normal skeletal development and were born in the expected Mendelian ratios. These results suggest that the entire *Pdk* family is dispensable for embryogenesis. Moreover, we show for the first time that in the absence of all PDK isoenzymes, PDC is still phosphorylated on site 2 (S300), implying the existence of a backup mechanism. Bioinformatic analysis implicated BCKDK, an enzyme that regulates the catabolism of branch chain amino acids, in this mechanism. Loss of site 2 phosphorylation and in utero death of the combined *Pdk*'s and *Bckdk* KO mice strongly support this possibility. Overall, we identify BCKDK regulation of PDC as a novel mechanism that can backup PDK family function to maintain embryonic development.

RESULTS

PDK1, PDK2 and PDK4 are dispensable for development and growth

To study in vivo the role of PDK family, we first focused on PDK1. Since the involvement of this isoenzyme in metabolic homeostasis was mostly studied in the context of cells under hypoxic conditions[14,15,33,34], we chose the hypoxic growth plate during mouse bone development as a model[24,25,28,29,35]. Using the knockout-first allele method, we generated three mouse strains: floxed-*Pdk1, Pdk1-lacZ* knockout (KO) and *Pdk1* KO (Fig. S1A). Examination of the *Pdk1-lacZ* KO reporter line verified strong *Pdk1* expression in developing bones of E14.5 embryos, including long bones, vertebrae and facial bones (Fig. S1B-C). Surprisingly, both homozygous *Pdk1-lacZ* KO and *Pdk1* KO mice had no apparent bone phenotype during embryonic development, as confirmed by skeletal preparation (Fig. 1C,D) and histological sections (Fig. 1E,F). These mice developed normally and produced viable and fertile colonies matching expected Mendelian ratios (Fig. 1G).

To understand the lack of phenotype, we examined the levels of different metabolites related to the TCA and glycolysis pathways in growth plate chondrocytes from *Pdk1* KO and control mice. Chondrocytes from tibiofemoral growth plates were extracted and grown in culture, and the TCA and glycolysis pathways were traced using ^{13}C isotopically labeled glucose. Results showed similar levels of metabolites (glucose, glutamine and glutamate) in control and *Pdk1* KO chondrocytes, indicating that metabolic homeostasis in those cells is maintained. Moreover, we detected similar levels of lactate, suggesting that a metabolic shift to enhanced glycolysis occurred in the absence of *Pdk1* (Fig. 1H).

A plausible explanation for the lack of phenotype in the absence of *Pdk1* is that other PDK isoenzymes compensated for its activity. Null mutants for *Pdk2* and *Pdk4* were reported to develop normally and have viable and fertile colonies [30,31]. Therefore, to examine the functional redundancy hypothesis, we generated double KO (dKO) and triple KO (tKO) mouse models lacking *Pdk1* and *Pdk2*, or *Pdk1* and *Pdk4*, or all three of these genes. The loss of these genes was verified by quantitative RT-PCR (qRT PCR) (Fig. S2A). Surprisingly, none of the combinations exhibited any bone phenotype (Fig. 1H-M). Moreover, *Pdk* tKO mice produced viable and fertile colonies matching expected Mendelian ratios (Fig. 1N). These outcomes indicated that PDK1, PDK2 and PDK4 are dispensable for bone and embryonic development.

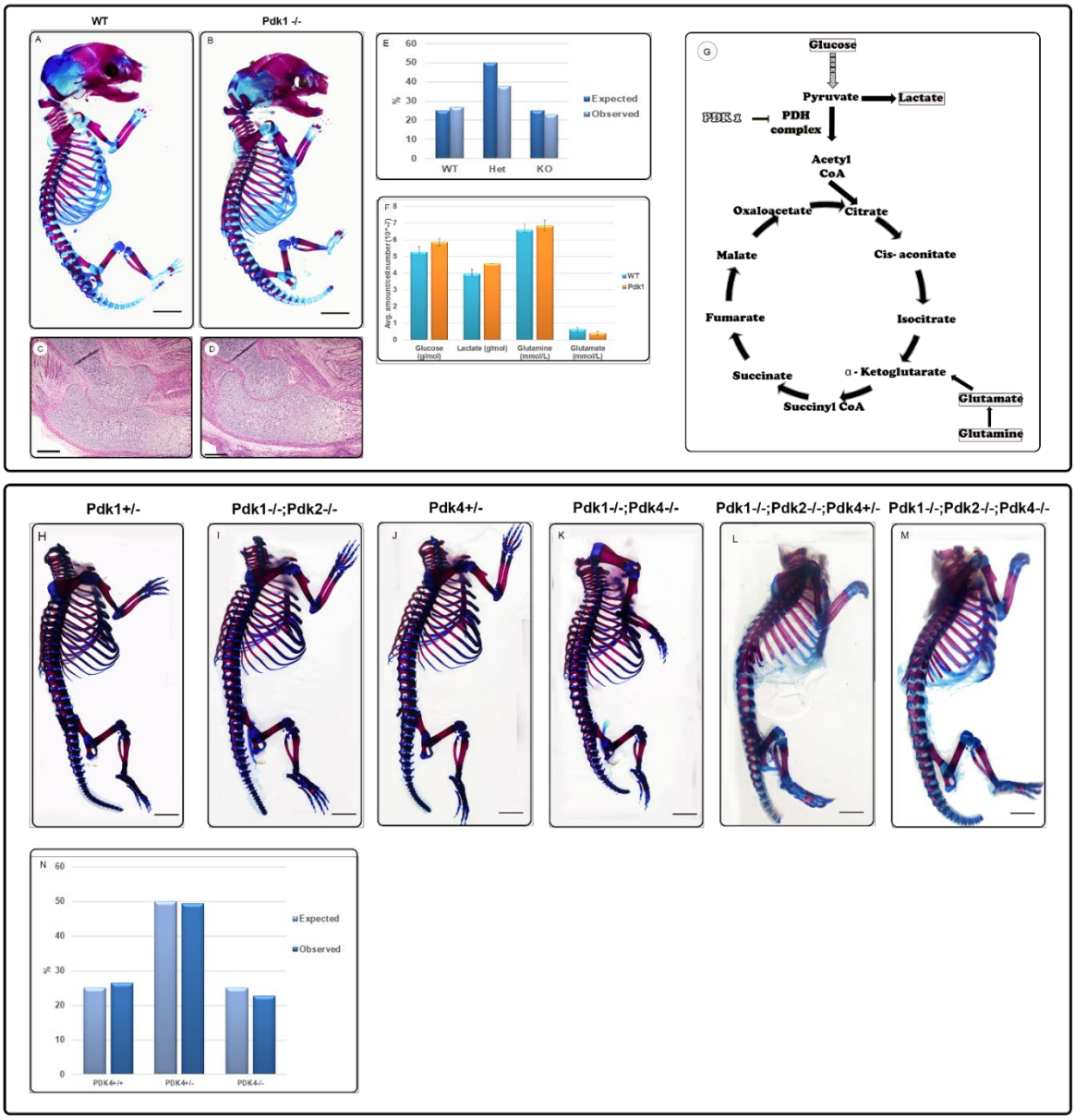

Figure 1. Deletion of single, double or triple *Pdk* genes in vivo does not affect embryonic development. (**A,B**) Skeletal preparations of control **(A)** and *Pdk1* KO **(B)** E17.5 embryos showing no skeletal phenotype (scale, 50 µm). (**C,D)** H&E staining of control and *Pdk1* KO E15.5 embryonic sections of olecranon and distal humerus growth plates (scale, 50 µm). **(E)** Graph showing expected Mendelian ratios of *Pdk1* KO progeny.

(F) Graph showing similar absolute levels of glycolysis-TCA pathway-related metabolites in chondrocytes from E17.5 *Pdk*1 KO and WT embryos (Nova analyzer, n=3). **(G)** Schematic illustration of the TCA cycle highlighting the relevant metabolites entry point to the cycle . **(H-M)** Skeletal preparations of control ($Pdk1^{+/-}$, H), *Pdk1-Pdk2* dKO (I), control ($Pdk4^{+/-}$, J) and *Pdk1-Pdk4* Dko (K), control ($Pdk1^{-/-}Pdk2^{-/-}$ $Pdk4^{+/-}$,l) and *Pdk1-Pdk2-Pdk4* tKO (M) newborn pups. (H and I, J and K, and L and M are littermates; scale, 50 µm). **(N)** Graph showing expected Mendelian ratios in colonies of *Pdk* tKO mice.

Loss of the *Pdk* family results in postnatal lethality due to hypoglycemia and ketoacidosis

The lack of phenotype in the *Pdk* tKO mice led us to study the only remaining candidate from the Pdk family, namely *Pdk*3. Recently, *Pdk*3 was also shown to be a HIF1α target under hypoxic conditions [18]. Thus, we hypothesized that *Pdk*3 might be sufficient to maintain normal embryonic development. Therefore, we established a genetic model in which the expression of all four *Pdk* genes is deleted. Using the CRISPR/Cas9 genome editing method, we targeted *Pdk3* gene on the genetic background of $Pdk1^{flox/-}Pdk2^{-/-}Pdk4^{-/-}$ mice. Considering the possible embryonic lethality, we established two independent lines. The first was of *Prx1-Cre;*$Pdk1^{flox/-}Pdk2^{-/-}Pdk3^{-/-}Pdk4^{-/-}$ mice to produce progeny of *Pdk* conditional quadruple knockout (cKO), lacking all *Pdk* genes in *Prx1*-expressing limb mesenchyme only. The second line was back-crossed to generate $Pdk1^{-/-}Pdk2^{-/-}Pdk3^{-/-}$ $Pdk4^{-/-}$ quadruple KO mice (total KO) (Fig. 3A).

Using qRT-PCR and western blot analysis on *Pdk* total KO mice, we verified deletion of all four *Pdk* genes at both mRNA and protein levels (Fig. 3B,C). Moreover, western blot analysis of chondrocytes derived from *Pdk* cKO growth plates showed deletion of PDK1

protein compared to cells from WT and control littermates, where *Prx1-Cre* was not present (Fig. 3D). The results indicated effective deletion of all four *Pdk* genes in both total KO and cKO mice. Surprisingly, skeletal preparation and histological sections from *Pdk* cKO mice revealed no bone phenotype (Fig. 3E-F'). Monitoring the colonies, we found that *Pdk* cKO mice produced viable and fertile colonies matching expected Mendelian ratios (Fig. 3G). Similarly, examination of bone development in skeletal preparation and histological sections of *Pdk* total KO embryos revealed no major skeletal phenotype (Fig. 3H-I'). However, although embryonic Mendelian ratios were observed as expected (Fig. 3J), this mouse strain did not produce viable colonies, as shown by the non-Mendelian ratios of mature mice colonies (Fig. 3K).

Examination of newborn *Pdk* total KO pups revealed that they died between P0 and P4. In light of *Pdk* loss of function, we assumed that a greater flux through the PDC might occur. This would lead to high utilization of glucose, followed by accumulation of acetyl CoA that can be used to synthesize ketone bodies[32], i.e. acetoacetate (AcAc), 3-β-hydroxybutyrate (3HB) and acetone. These are produced by the liver and used peripherally as an energy source when glucose is not readily available[36]. Since synthesis of ketone bodies from glucose is largely prevented by the phosphorylation and inactivation of PDC[32], loss of the *Pdk* family should elevate their production[32]. Indeed, when we analyzed the serum of P1 *Pdk* total KO mice, we found significantly higher 3HB levels and lower glucose levels as compared to WT mice (Fig. 3L). Deeper metabolic profiling of serum composition from these mice showed significantly low levels of pyruvate and lactate together with a higher utilization of acetyl CoA, reflected by higher levels of acetoacetate and 3HB, reduced production of the more distal TCA metabolites, and high levels of branched chain amino acids (BCAA) (Fig. 3M). These results are consistent with the

expected effect of *Pdk* loss [32,37], and suggest that the cause of the early postnatal death was ketoacidosis and hypoglycemia. Together, these results suggest that *Pdk* family is dispensable for embryonic development but is necessary postnatally to maintain energy metabolic balance.

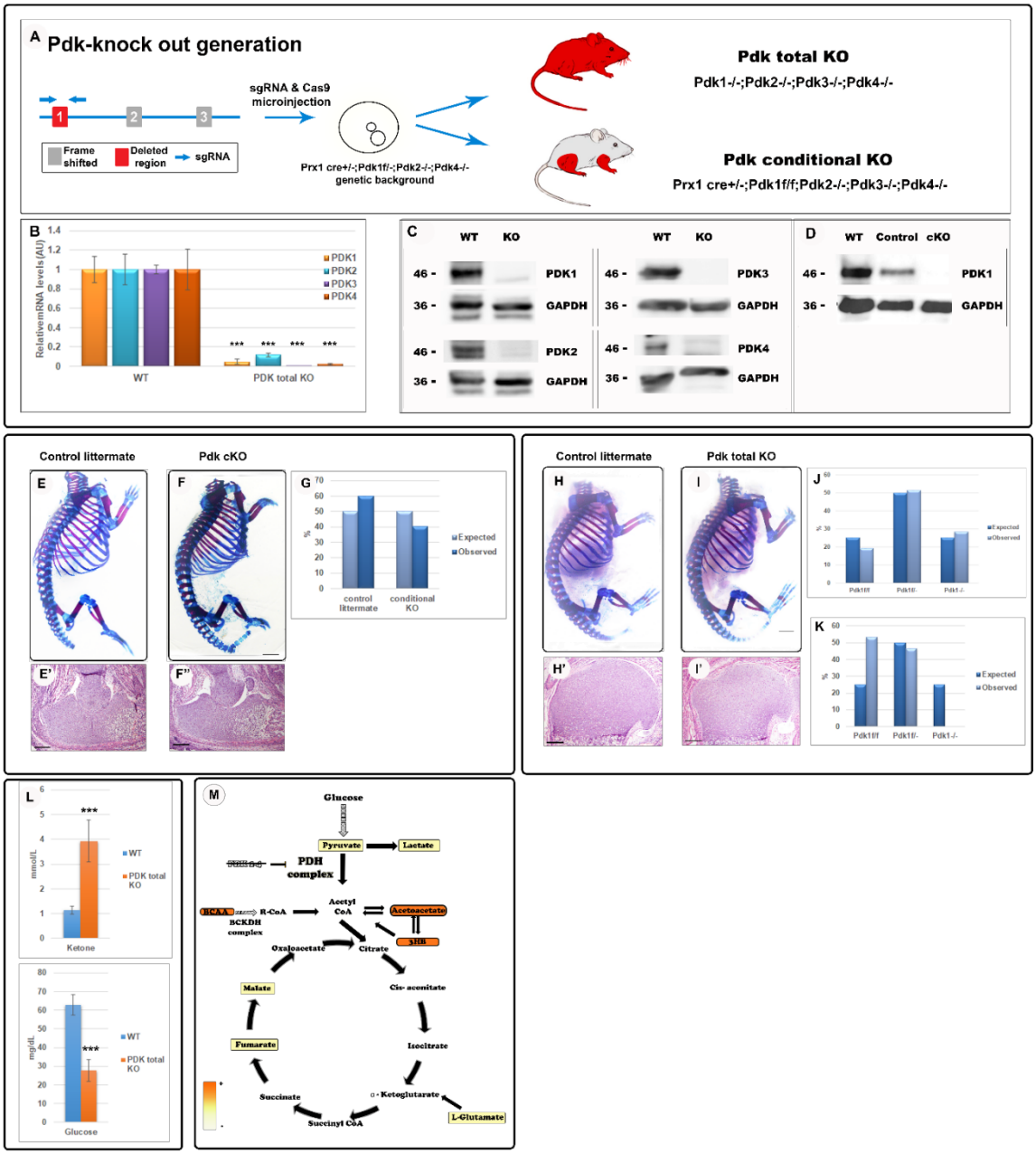

Figure 3. Deletion of the entire *Pdk* family results in normal embryonic development followed by postnatal lethality. (A) Schematic representation of *Pdk3* gene and the targeted site of CRISPR/Cas9-mediated deletion. This was followed by zygote injection to generate *Pdk* total KO mice or *Pdk* conditional KO in limb mesenchyme only, depending on the genetic background. **(B)** qRT-PCR of *Pdk* mRNA confirms deletion of all four genes, as compare to WT (***, $P<0.0001$; $n=4$ for each

genotype; data are normalized to *Tbp* and presented as mean±SD). **(C)** Protein expression analysis of four PDK isoenzymes, derived from hearts of *Pdk* total KO or WT P0 pups, shows complete deletion of the entire PDK family (representative images, *n*=3). **(D)** Protein expression of PDK1 in chondrocytes from *Pdk* cKO, control littermate and WT embryos shows deletion of PDK1 in the mutant (representative images, 3 biological repeats, *n*=5 for each sample). **(E-F')** Skeletal preparations (E,F) and H&E staining of olecranon and distal humerus sections (E',F') from E18.5 *Prx1-Cre;Pdk1*$^{f/f}$*;Pdk2*$^{-/-}$;*Pdk3*$^{-/-}$;*Pdk4*$^{-/-}$ embryos and control littermate (without Cre) show that the *Pdk* cKO embryos develop normally (scale, 100 µm). **(G)** Graph showing expected Mendelian ratios in *Pdk* cKO progeny. **(H-I')** Skeletal preparations at E18.5 (H-I) and H&E staining (H',I') of sections from P0 *Prx1-Cre;Pdk1*$^{f/-}$;*Pdk2*$^{-/-}$;*Pdk3*$^{-/-}$;*Pdk4*$^{-/-}$ mice and control littermate show that the *Pdk* total KO embryos develop normally (scale, 100 µm). **(J)** Graph showing expected Mendelian ratios in embryos of *Pdk* total KO mice. **(K)** Graph showing non-Mendelian ratios in colonies of mature *Pdk* total KO mice, as a result of loss of the total KO genotype. **(L)** Graphs showing blood levels of glucose and 3HB, a ketone body, in *Pdk total* KO P1 pups, compared to WT pups. Data are presented as mean ± SD; $P<0.0001$; $n_{WT}=9$; $n_{KO}=4$). **(M)** Scheme of P1 serum metabolic profiles of *Pdk* total KO pups by LC-MS polar metabolite analysis. Higher levels are shown in orange and lower levels in yellow, as compared to WT levels ($P<0.05$; fold change >2, $n_{WT}=4$; $n_{KO}=3$).

PDC phosphorylation on site S300 is maintained upon PDK family loss of function

To gain molecular insight into the apparently normal development of the *Pdk* total KO embryos, we studied the three phosphorylation sites on PDHA1, which regulate PDC activity. First, we examined by western blot analysis PDC phosphorylation sites in cultured chondrocytes isolated from *Pdk* cKO growth plates. Interestingly, we found that one of the three sites, namely S300, was phosphorylated (Fig. 4A). To rule out the possibility that the phosphorylation of site S300 resulted from the presence of PDK1 from surrounding tissues, such as skeletal muscles, we produced mouse embryonic fibroblasts (MEFs) from the total *Pdk* KO mice. As seen in Fig. 4B, site S300 was phosphorylated in these MEFs as well. These results suggest the existence of a backup mechanism that phosphorylates and inactivates PDC in the absence of all four PDKs.

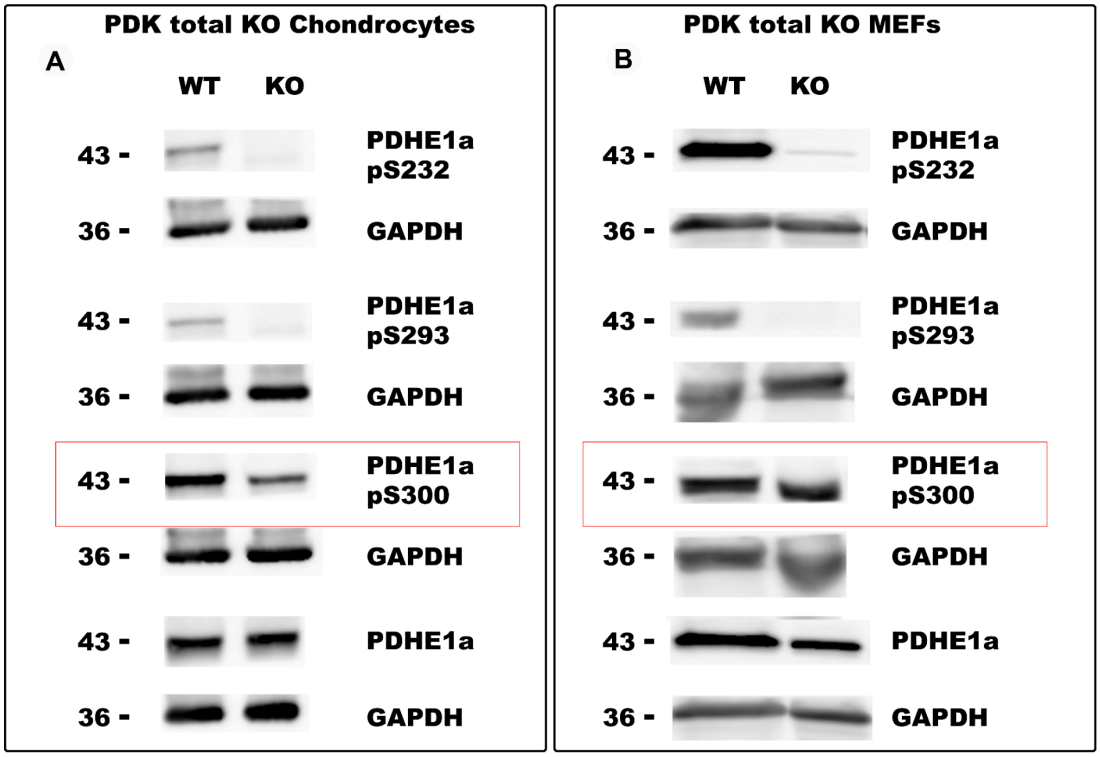

Figure 4. PDC phosphorylation on site 2 (S300) is PDK independent. (A,B) Western blot analysis of the three PDC phosphorilation sites in chondrodytes extracted from E17.5 growth plates of *Pdk* cKO embryos (A; *Prx1-Cre*$^{+/-}$*Pdk1*$^{flox/flox}$*Pdk2*$^{-/-}$*Pdk3*$^{-/-}$*Pdk4*$^{-/-}$*)* and MEFs derived from *Pdk* total KO embryos (B), compared to WT. As controls, PDHA1 and endogenous GAPDH total protein levels were measured. Each chondrocyte sample is a pool of 5 biological repeats; *n*=3 for all groups. Red squares indicate active phosphorilation on site S300.

***Bckdk* is necessary for embryonic development in the absence of *Pdk* family**

Our results suggested that another kinase, which is not a Pdk, phosphorylates PDC on site S300. To identify this kinase, we searched for suitable candidates using bioinformatic tools such as, Ensemble[38], GeneCards [39]. One candidate that emerged was branched chain ketoacid dehydrogenase kinase (Bckdk), which catalyzes the phosphorylation and inactivation of the branched-chain alpha-ketoacid dehydrogenase complex (BCKDC), the key regulatory enzyme of the valine, leucine and isoleucine catabolic pathways[40]. GenesLikeMe analysis [41] predicted that Bckdk was a paralog of *Pdk*1 and belonged to the same mitochondrial kinase proteins family, mainly by sequence and domain similarity (Fig. 5A and Fig. 2S). Moreover, protein-protein interaction analysis by STRING [42] predicted BCKDK to interact with PDHA1 subunit, thus possibly mimicking the kinase activity of PDK and inhibiting PDC activity (Fig. 5B).

Based on these observations, we hypothesized that *Bckdk* serves as the backup mechanism for Pdk family during embryonic development. To test our hypothesis, we sought to delete *Bckdk* in mice that lack all *Pdk* genes in limb mesenchyme and examine PDC phosphorylation. *Bckdk* KO mice was previously reported to be viable and to display

postnatal growth retardation[43]. Utilizing the CRISPR/Cas9 method, we generate a *Bckdk* KO mouse strain on the background of *Prx1-Cre-Pdk1*^{floxflox}*Pdk2*$^{-/-}$*Pdk3*$^{-/-}$*4*$^{-/-}$ (*Pdk* cKO-*Bckdk* KO) (Fig. 5C). The deletion of *Bckdk* gene in these mice was verified at both mRNA and protein level by qRT-PCR and western blotting, respectively (Fig. 5D,E). Crossing the heterozygous *Pdk* cKO-*Bckdk* KO mice, we failed to acquire the predicted Mendelian ratio of embryos at E12.5, which indicates embryonic lethality. At E10.5, a stage at which the *Prx1-Cre* is activated [44], genotype distribution of *Pdk* cKO-*Bckdk* KO embryos was closer to the expected Mendelian ratios (Fig. 5F). Yet, some of these embryos displayed developmental regression in comparison to control littermates (Fig. 5G). Taken together, these results strongly support the hypothesis that Bckdk compensates for the absence of PDK isoenzymes during development.

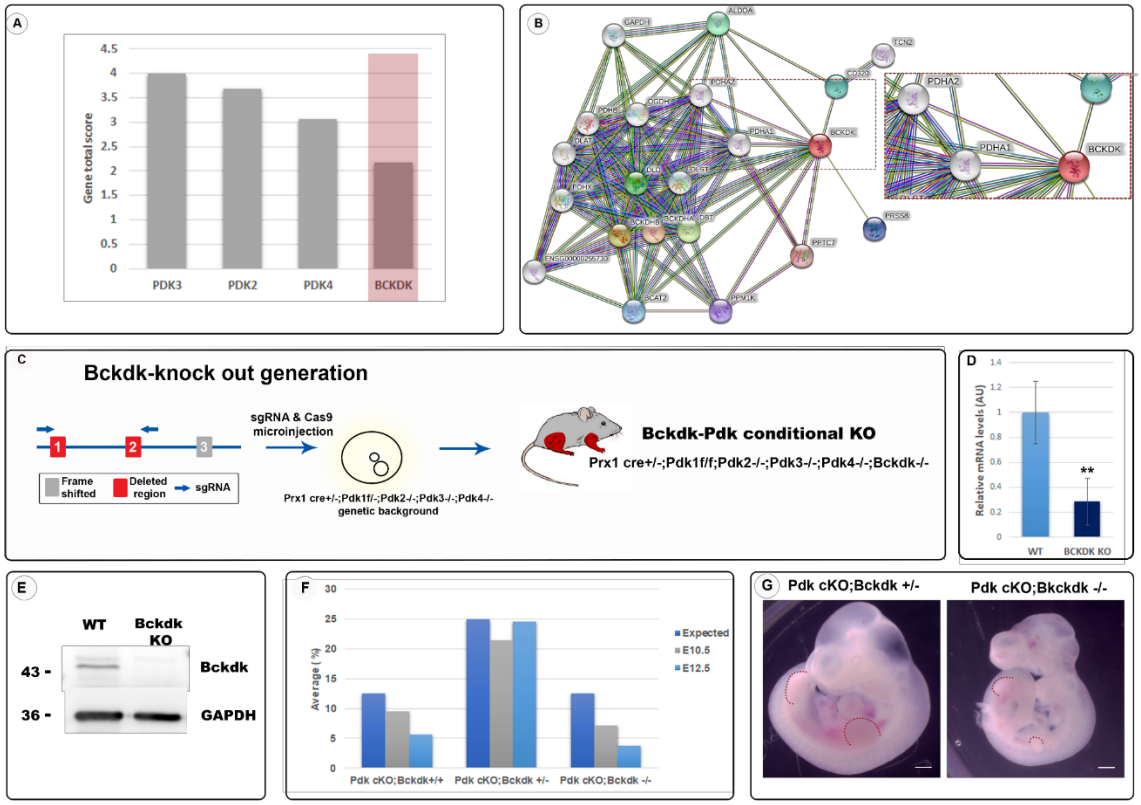

Figure 5. *Pdk* cKO-*Bckdk* KO mice display embryonic lethality. (A) GenesLikeMe analysis identifies *Bckdk* as a *Pdk1* paralog, along with the other *Pdk* family members (total score combines sequences, domains, super pathways, expression, compounds and gene ontology similarities). **(B)** STRING analysis predicts protein-protein interaction between BCKDK and PDH complex subunit PDHA1 (string legend: yellow, textmining; black, co-expression; pink, experimentally determined). **(C)** Schematic representation of *Bckdk* gene and the targeted sites of CRISPR/Cas9-mediated deletion. This was followed by zygote injection to generate *Pdk* cKO-*Bckdk* KO in limb mesenchyme only. **(D)** qRT-PCR of *Bckdk* mRNA in *Pdk* cKO-*Bckdk* KO mice, as compare to WT (**, P<0.001; *n*=3 for each genotype; data normalized to *Tbp* and presented as mean±SD. **(E)** Protein expression analysis by western blotting shows complete deletion of BCKDK in *Pdk* cKO-*Bckdk* KO

mice (*n*=3) **(F)** Mendelian ratios of *Pdk* cKO-*Bckdk* KO mutant at E12.5 (n=106) and E10.5 (n=42) embryos; data are shown as percentage from Cre-positive embryos only. **(G)** Representative E10.5 *Pdk* cKO-*Bckdk* KO embryo displays delayed development as compared to control *Bckdk* heterozygous littermate (dashed red lines indicate the limbs; scale, 50 μm).

***Bckdk* is necessary for PDC phosphorylation in *Pdk* loss-of-function mice**

To further strengthen our hypothesis, we sought to test directly if *Bckdk* is necessary for PDC phosphorylation on site S300 in the absence of all *Pdk* family members. To overcome the early embryonic lethality of mice lacking all *Pdk* genes and *Bckdk*, we used the $Pdk1^{flox/flox}$ allele to generate embryos that lack *Pdk2, Pdk3, Pdk4* and *Bckdk* but still have the intact *Pdk1* ($Pdk1^{flox/flox}Pdk2^{-/-}Pdk3^{-/-}Pdk4^{-/-}Bckdk^{-/-}$). Next, these embryos were used to generate primary MEF cultures. We then infected these cells with adeno-Cre virus to ablate the expression of *Pdk1*, or with adeno-GFP as a control. As seen in Figure 6, PDK1 protein expression level was reduced in adeno-Cre-infected $Pdk1^{floxflox}Pdk2^{-/-}Pdk3^{-/-}Pdk4^{-/-}Bckdk^{-/-}$ cells. Concomitantly, PDC phosphorylation on S300 site was strongly reduced in these cells.

The infection of MEFs with adeno-Cre virus resulted in low levels of PDK1 expression, which correlated with low phosphorylation on PDC S300 site. Therefore, to inhibit the activity of the remaining PDK1, we added to the culture dichloroacetate (DCA), a PDK inhibitor[45]. As seen in Figure 6, DCA nearly eliminated PDK1 function and blocked the phosphorylation of site S300. Collectively, these results provide, for the first time, strong molecular evidence to the ability of BCKDK to regulate PDC and act as a backup mechanism for the PDK family by catalyzing phosphorylation of site S300.

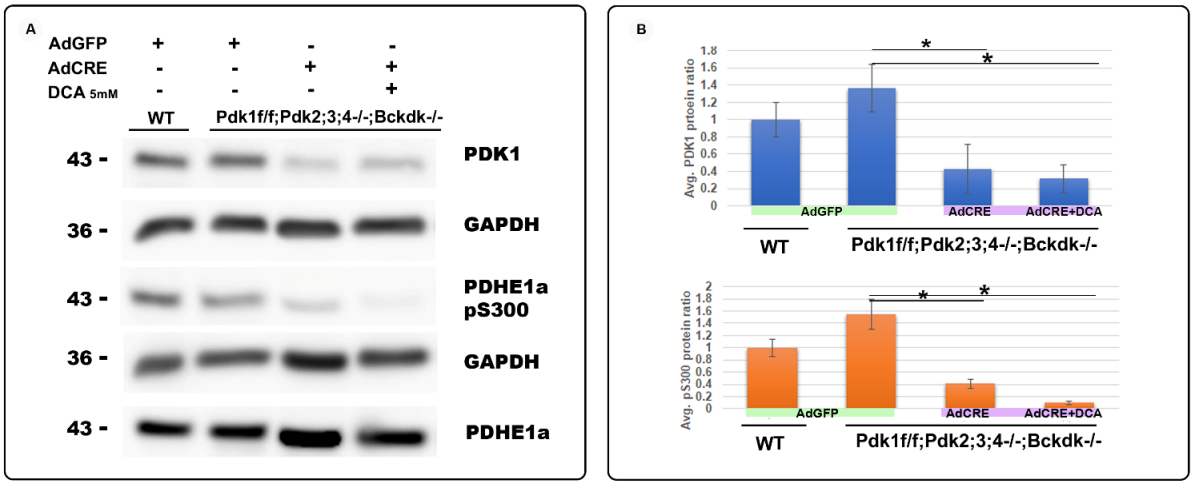

Figure 6. PDC phosphorylation on site S300 is BCKDK dependent. **(A)** Western blot for PDK1 and phosphorylated S300 site (pS300) on PDHA1 in MEFs derived from *Pdk1*$^{flox/flox}$*Pdk2*$^{-/-}$*Pdk3*$^{-/-}$*Pdk4*$^{-/-}$*Bckdk*$^{-/-}$ mice and infected with either Adeno-GFP as a control, or Adeno-CRE with or without addition of 5 mM DCA, to ablate PDK1 (representative images) **(B).** Graphs showing mean levels of PDK1 (top) and pS300 (bottom) in cells treated with adeno-Cre with or without DCA, relative to their levels in WT or control cells infected with Adeno-GFP. n=3, $P<0.05$).

DISCUSSION

The ability of cells to adapt to different environmental conditions and maintain energetic homeostasis is one of the hallmarks of life. Using oxygen as the most common electron acceptor allows cells to maximize utilization of acetyl CoA driven from three catabolic pathways of glucose, amino acids and fatty acids feeding the TCA cycle. In this work, we discover a novel regulatory metabolic circuit between glucose and BCAA catabolic pathway. We found that BCKDK, a key regulator of BCAA catabolic pathway, regulates the activity of PDC, the gatekeeper of the glucose catabolic pathway. As the underlying mechanism, we show that phosphorylation of PDC on its serine residue S300 of PDHA1 is BCKDK dependent. This finding reveals a new backup mechanism for the PDK family in regulating PDC activity, which allows cellular metabolic balance to sustain embryonic development (Fig. 7).

BCAAs are a group of indispensable amino acids that includes leucine, isoleucine, and valine[43]. Their catabolism serves the cellular energetic balance by feeding the TCA cycle through a two-step degradation pathway of transamination to form branched chain α-keto acids (BCKAs), followed by oxidation and decarboxylation resulting in an irreversible synthesis of acetyl-CoA entering the TCA cycle[46]. The second step is crucial for degradation by BCKDC multienzyme. Therefore, BCKDC regulation is important to maintain proper levels of BCAAs and normal development[43]. Interestingly, PDC and BCKDC share many structural and enzymatic properties, as well as mechanism of regulation. Similarly to PDC, BCKDC is regulated by reversible phosphorylation of its E1 subunit on two serine sites (ser293 and ser303) mediated by its own native kinase, BCKDK. The activity of the entire BCKDC complex depends on BCKDK function, which is regulated by a feedback loop of substrate metabolites, e.g. BCAA blood levels [47].

Over the years, an interplay between the glucose and BCAA catabolic pathways has been established [46]. Recently, it was shown that these pathways can regulate one another through feedback loops of the source nutrients circulation, i.e, glucose and amino acids, to maintain energetic balance. Excessive or insufficient levels of glucose or BCAAs was shown to influence transcription of elements of the parallel pathway. For example, BCAA levels can improve glucose uptake by upregulation of glucose transporters [48], and a reciprocal effect was shown when glucose levels are high[49]. Our discovery that BCKDK can phosphorylate PDC on site S300 uncovers a new level of regulation that hardwires glucose and BCAA degradation pathways through direct enzymatic regulation and not by a feedback loop of circulating nutrients.

From an evolutionary viewpoint, Oppenheim et. al [50] recently showed that in some parasites lacking mitochondrial PDC, acetyl-CoA is converted from pyruvate by BCKDC, which fulfills PDC function. Therein, it was suggested that BCKDC evolved earlier than PDC. Although the ancestral gene of the regulators of these complexes, i.e. *Pdk* and *Bckdk,* is yet to be discovered, sequence similarities between *Pdk* and *Bckdk* has placed them as paralogs belonging to the same mitochondrial kinase family[51–54]. Here, we provide strong in vivo evidence suggesting that *Bckdk* is not only a paralog, but also a functional paralog of the *Pdk* family. One interesting question that remains is whether BCKDK acts only as a backup mechanism for the loss of the PDK family, or is it a part of PDC regulation in normal conditions as well. Another intriguing question that is raised by the observed functional compensation is whether PDKs can compensate for the absence of BCKDK. This assumption makes sense considering that *Bckdk* KO mice are viable and exhibit growth retardation only at three weeks of age, due to lack of BCKDC regulation[43].

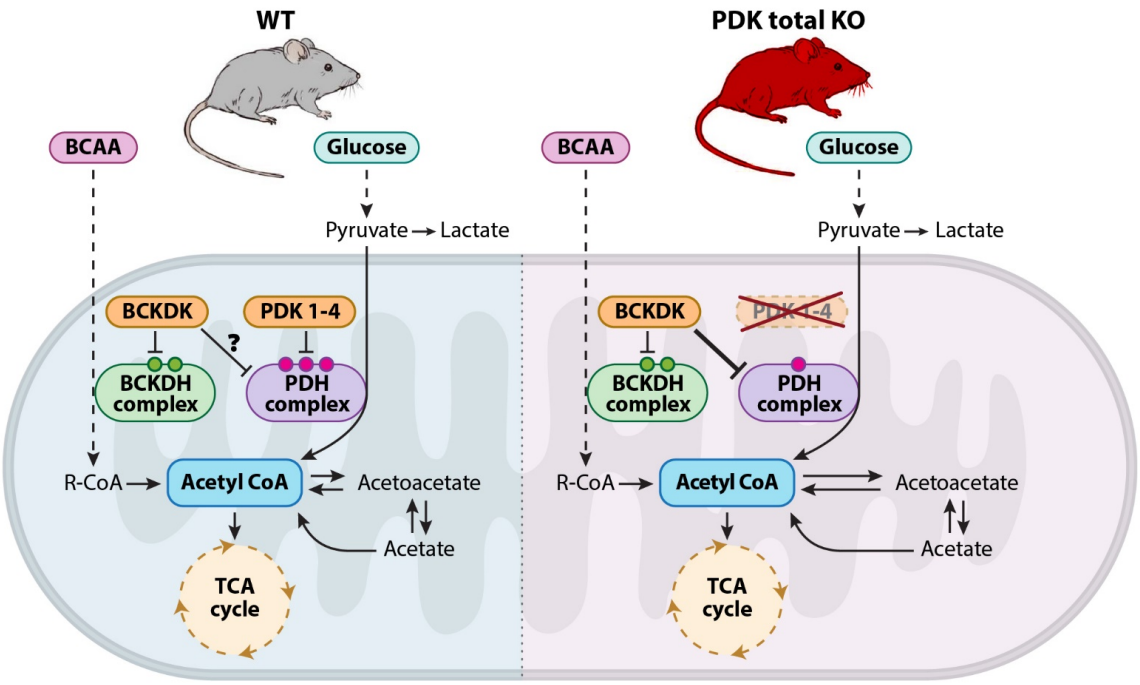

Figure 7. BCKDK compensates for *Pdk* loss of function via PDC site S300 phosphorylation. Cartoon depicting the interplay between glucose and BCAA catabolism in WT (left) versus *Pdk* total KO mice (right). In WT mice, PDC is inactivated by phosphorylation on three serine residues, whereas in the *Pdk* total KO mice, only site 2 (S300) is phosphorylated in a *Bckdk*-dependent manner. This novel level of regulation implicates BCKDK as a functional paralog of the PDK family, which may also act in the same way in the presence of PDKs.

Our *Pdk* loss-of-function in vivo model provided us with an opportunity to address the question of PDC site specificity. While there are studies showing that phosphorylation of only one of the three sites can cause complete inactivation[4,55,56], others provide indications for phosphorylation site specificity[57]. For example, it was shown that each phosphorylation site is regulated by a different PDK isoenzyme[7,58] in a tissue-specific manner[52]. Moreover, while phosphorylation on site 1 (S293) blocks the access to PDC active site[55] and is more

rapid[59], the function of sites 2 (S300) and 3 (S232) is less understood and was suggested to cause only a delay in reactivation of PDC[7,57]. Our in vivo study shows that BCKDK can only regulate the phosphorylation of site 2, which was sufficient to support embryonic development, but not for postnatal growth. These findings support the notion of different roles of the three sites, and may suggest another, yet undescribed role for site 2 specificity. It would be interesting to further study in vivo the roles of the different phosphorylation sites of PDC and their effect on the metabolic balance.

Another level of specificity in the regulation of PDC is related to the different expression patterns of PDK isoenzymes, which are known to be tissue-specific[52]. Another indication is the fact that only PDK1 can phosphorylate all three sites of PDC[7,58]. Moreover, each isoenzyme was shown to be regulated by different physiological conditions [5,9,10] By contrast, several studies support the possibility of functional redundancy among the PDK family members, for example, between *Pdk1* and *Pdk2* in muscle tissue in vitro [30] and between *Pdk2* and *Pdk4* iv vivo [32]. Our findings that loss of function of different *Pdk* genes did not affect development in mice increases the scope of known functional redundancy among these four isoenzymes. The sequential targeting of these genes demonstrates that each PDK can compensate for the loss of the other family members. This obviously raises the need to conduct physiological studies and test this redundancy under challenging conditions.

On that note, hypoxic conditions have long been associated with pathologies , such as tissue ischemia, inflammation and cancer[60]. However, hypoxic microenvironments were shown to be essential for mammalian embryonic development[23]. In either state, HIF1 transcription factor initiates a key molecular response that maintains O_2 homeostasis and metabolic balance[14,21]. Specifically, the HIF1α-PDK axis is considered a major regulator of cell

adaptation to hypoxia by both controlling energy production and decreasing mitochondrial oxygen consumption[12–14,16,18,61]. However, our results of normal development in the absence of one side of this axis, namely all PDKs, question its significance. There are three possibilities to reconcile our findings with the common view. One is that HIF1α activation of a wide range of downstream target genes is adaptive enough to support metabolic energy balance under hypoxia even without inactivation of PDC. For example, by activating pyruvate kinase isoform M2), which diverts pyruvate to the pentose phosphate pathway [18]. Second, it is possible that by activating another, yet undescribed mechanism, HIF1α compensates for the absence of PDK family. In that context, the possibility that HIF1α can regulate *Bckdk* should be considered. Finally, it is possible that the involvement of HIF1α-PDK axis is restricted to the development or function of specific organs, which are dispensable for embryonic development. In support of this explanation is our finding that mice lacking all *Pdk* genes in limb mesenchyme developed normally, whereas total *Pdk* KO mice died at early neonatal stages. The metabolic abnormalities in these newborn total KO mice strongly imply that the affected organs are involved in physiological regulation of the organism, which is critical for its survival postnatally but not during embryogenesis. It is also possible that during development, the consequences of metabolic abnormalities, such as ketone body accumulation and hypoglycemia, are buffered by the safe environment of the placenta[62]. Obviously, the different outcomes of embryonic development and postnatal growth of *Pdk* total KO mice does not exclude the possibility that these two processes have different metabolic requirements. In that case, it is possible that BCKDK could backup for PDKs only during the embryonic period.

To conclude, our findings provide new insight into the functional redundancy among PDK family members in modulating PDC activity to maintain energy production and cell

survival, while revealing the existence of a previously unknown backup mechanism, which places *Bckdk* as a functional paralog of *Pdk*. This backup mechanism unveils a new level of regulatory crosstalk between two central metabolic pathways that feed the TCA cycle. The finding of this backup mechanism may promote the development of new therapeutic strategies for complex diseases involving changes in the metabolic state of cells, such as cancer, diabetes and many other metabolic diseases.

MATERIALS AND METHODS

Animals. Mice were monitored daily by staff and veterinary personnel for health and activity. Mice were given ad libitum access to water and standard mouse chow with 12-hr light/dark cycles. All animal procedures were approved by the Institutional Animal Care and Use Committee and performed in strict adherence to Weizmann Institute Animal Care and Use guidelines, following the NIH, European Commission, and Israeli guidelines. In all timed pregnancies, plug date was defined as E0.5. For harvesting of embryos, timed-pregnant female mice were sacrificed by CO_2 intoxication. The gravid uterus was dissected out and suspended in a bath of ice-cold PBS and the embryos were harvested. Tail genomic DNA was used for genotyping.

Generation of *Pdk1*, *Pdk2, Pdk4* knockout mice. The generation of *Pdk2* KO [30] and *Pdk4*-KO mice [31] was previously described. For the generation of *Pdk1* KO mice, embryonic stem cells with a gene trap insertion (KO-first allele) in the *Pdk1* gene were obtained from the European Conditional Mouse Mutagenesis program (EUCOMM)[63]. *Pdk1* KO mice were crossed with PGK-Cre^{m} mice[64] to generate the null *Pdk1-lacZ* mice. Alternatively, *Pdk1* KO mice were crossed with *Rosa26-FLPe* mice (Jackson laboratory, 016226) to generate the floxed-*Pdk1* mice. Genotyping of *Pdk1* KO, *Pdk1-lacZ* and floxed-*Pdk1* mice was performed by PCR (primer sequences are shown in Supplementary Table S1). Generation of double and triple KO combinations of *Pdk1*, *Pdk2* and *Pdk4* was done by strain breeding.

CRISPR/Cas9 generation of *Pdk3* and *Bckdk* KO. Cas9 plasmid and plasmids encoding guide RNAs were designed using several CRISPR designing tools and optimized for the best guides, including: the MIT CRISPR design tool [65] and sgRNA Designer, Rule Sets 1 and 2 [66,67], in both the original sites and later in the Benchling implementations

(www.benchling.com), SSC [68], and sgRNAscorer [69], in their websites. The following oligos were used for construction of gRNA: *Pdk3*: 5'-CGGGTTGGGGAGGTCTAGAG-3' (an upstream above the putative TSS) and 5'-ATTCCGTGAGAAGCTCCGGG-3' (downstream of the ATG in the first exon), total deletion of 560 bp (location X:93831603-93832603). For *Bckdk*: 5'-CCCGCGCGATGTTACAGCCG-3' (an upstream guide around the TSS and 5'-CTCTACATGGTGTGTATCGG-3' (downstream of the ATG in the second exon), total deletion of 884bp (location chr7:127903907-127905206). In vitro transcribed Cas9 RNA (100 ng ml 1) and sgRNA(50 ng ml 1) were injected into one-cell stage fertilized embryos isolated from superovulated *Prx1-Cre;Pdk1*$^{flox/-}$*Pdk2*$^{-/-}$*Pdk4*$^{-/-}$ or *Prx1-Cre;Pdk1*$^{flox/-}$*Pdk2*$^{-/-}$*Pdk3*$^{-/-}$*Pdk4*$^{-/-}$ mice mated with males of the same mutation for generation of *Pdk* total KO and *Pdk* cKO- *Bckdk* KO, respectively. Injected embryos were transferred into the oviducts of pseudopregnant ICR females as previously described [70]. Genomic DNA from treated embryos was analyzed by PCR primers designed to verify the deleted sequence of each gene; primer sequences are shown in Supplementary Table S1.

Histology. For hematoxylin and eosin staining, embryos were fixed overnight in 4% paraformaldehyde (PFA) – phosphate-buffered saline (PBS), decalcified in a solution containing equal parts of 0.5 M ethylenediaminetetraacetic acid (EDTA; pH 7.4) and 4% PFA in PBS overnight, dehydrated to 100% ethanol, embedded in paraffin and sectioned at a thickness of 7 μm. H&E staining was performed following standard protocols.

X-gal staining. Whole-mount X-gal staining was performed as described previously[71].

Skeletal preparation. Cartilage and bones in whole mouse embryos or newborn pups were visualized after staining with Alcian Blue and Alizarin Red S (Sigma) and clarification of soft tissue with potassium hydroxide [72].

Chondrocyte primary culture. For chondrocyte primary culture, hindlimbs of either E17.5 *Pdk1* KO or *Prx1-Cre;Pdk1*$^{flox/-}$*Pdk2*$^{-/-}$*Pdk3*$^{-/-}$*Pdk4*$^{-/-}$ and control WT embryos were dissected and soft tissue, skin and particularly muscles were removed. The growth plates were dissected and placed in DMEM 4500 mg/l glucose (Invitrogen) with 1% pen-strep solution (Biological Industries). Growth plates were digested in trypsin containing 0.25% EDTA (Biological Industries) for 30 minutes at 37°C and in 1 mg/ml collagenase type V (Sigma) in DMEM 4500 mg/l glucose with 1% pen-strep solution for 2 hours. Chondrocytes were plated at a density of $125x10^3$ cells/ml and grown under normoxia in monolayer cultures in high glucose DMEM supplemented with 10% fetal bovine serum (FBS, Biological Industries) and 1% pen-strep solution for 5 days until confluency (>90%).

Tissue culture and viral infection. Mouse embryonic fibroblasts (MEFs) were extracted from E12.5-14.5 *Pdk* total KO or *Pdk1*$^{flox/flox}$*Pdk2*$^{-/-}$*Pdk3*$^{-/-}$*Pdk4*$^{-/-}$*Bckdk*$^{-/-}$ and WT embryos, and cultured under normoxic conditions in DMEM (Gibco), 20% fetal calf serum, 1% L-glutamine, 1% penicillin/ streptavidin and sodium pyruvate. At passage 3 or 4, cells were taken either for qRT-PCR or western blot analysis. For adeno-viral infection, cells were infected with 300 viral particles/cell of Ad5CMVeGFP or Ad5CMVCre-eGFP virus (Gene Transfer Vector Core, University of Iowa). Then, cells were harvested for western blot analysis. During all experiments, medium was changed daily.

Glucose, glutamine, glutamate and lactate measurements. Chondrocytes were plated as described above. Upon reaching 80-90% confluency, cells were washed and incubated in a glucose- and glutamine-free DMEM medium supplemented with 10% dialysed serum, 4 mM L-glutamine (98% atom 13C5 95% (CP), Sigma 605166) and 10 mM D-[1,6-13C]-glucose (U-13C6, 99%+, Cambridge Isotope Laboratories, Inc.) or in the corresponding medium containing non-labelled L-glutamine and D-Glucose, for 12 h. Subsequently, 500 μL medium from the cell culture was collected, briefly centrifuged and directly injected into the Nova chemical analyzer. Background metabolite measurements from cell-free culture were subtracted, and results were normalized to cell number.

Quantitative real-time (qRT-) PCR. Total RNA was purified from either MEFs or chondrocyte primary culture using the RNeasy Kit (Qiagen). Reverse transcription was performed with High Capacity Reverse Transcription Kit (Applied Biosystems) according to the manufacturer's protocol. qRT-PCR was performed using Fast SYBR Green master mix (Applied Biosystems) on the StepOnePlus machine (Applied Biosystems). Values were calculated using the StepOne software version 2.2, according to the relative standard curve method. Data were normalized to TATA-box binding protein (*Tbp*) or 18S rRNA. Primer sequences are shown in Supplementary Table S2. Statistical significance was determined by Student's *t*-test as $P<0.05$.

Western blot analysis. For western blotting, protein was extracted from long bone growth plates of E17.5 embryos or from primary chondrocytes or MEFs as described above. Protein concentration was determined by Pierce protein BCA assay kit (Cyanagen). The following antibodies were used: PDK1 (AB202468, Abcam) PDK2, PDK3, PDK4, (AP7039b, AP14274b, AP7041b, Abgent), BCKDK (AB111716, Abcam), PDHe1 (AB110334, Abcam), PDHe1α S300 (AP1064, Calbiochem), PDHe1α S232 (AP1063,

Calbiochem), PDHE1α S293 (AP1062, Calbiochem) and GAPDH (AM4300, Ambion), followed by the appropriate HRP conjugated secondary antibodies (1:10,000; Jackson ImmunoResearch) and HRP detection using the EZ-ECL kit (Biological Industries).

Bioinformatic analysis of potential *Pdk* paralogs. GenesLikeMe paralog analysis (https://www.genecards.org/) for *Pdk1* was performed as previously described [41]. Protein-protein interaction analysis was done using STRING [42].

Liquid chromatography–mass spectrometry (LC-MS) polar metabolite analysis. Metabolic profiling of polar phase was done as described by Zheng et al.[73], with minor modifications. Briefly, analysis was performed using Acquity I class UPLC System combined with mass spectrometer (Thermo Exactive Plus Orbitrap), which was operated in a negative ionization mode. The LC separation was done using the SeQuant Zic-pHilic (150 mm × 2.1 mm) with the SeQuant guard column (20 mm × 2.1 mm) (Merck). Mobile phase A was acetonitrile, and Mobile phase B was 20 mM ammonium carbonate plus 0.1% ammonia hydroxide in water. The flow rate was kept at 200 µl min−1 and gradient was as follow: 0 -2 min 75% of B, 17 min 12.5% of B, 17.1 min 25% of B, 19 min 25% of B, 19.1 min 75% of B, 19 min 75% of B. Data processing was done using TraceFinder Thermo Fisher software, detected compounds were identified by Retention time and fragments and verified using in-house mass spectra library. Metabolic pathways analysis was done using Metacyc database [74].

ACKNOWLEDGMENTS

We thank Nitzan Konstantin for expert editorial assistance, Dr Robert Harris from the Indiana University which kindly provided us with PDK2 and PDK4 mice, Dr Nicola Brunetti-Pierri from the Telethon Institute of Genetics and Medicine for his support and

advice, Dr Ron Rotkoff for his help with statistical analysis, Dr Tsviya Olender for bioinformatics advice, and Neria Sharabi from the Department of Veterinary Resources for his help with mice maintenance. Special thanks to all members of the Zelzer Laboratory for encouragement and advice.

REFERENCES

1. Harris, R. A., Bowker-Kinley, M. M., Huang, B. & Wu, P. Regulation of the activity of the pyruvate dehydrogenase complex. *Adv. Enzyme Regul.* **42**, 249–259 (2002).

2. Tracy, B. Y., Flora, C. L. & Reed, L. J. REGULATION OF THE ACTIVITY OF THE PYRUVATE MITOCHONDRIA BY PHOSPHORYLATION AND DEPHOSPHORYLA TION *. 234–241 (1968).

3. O.H., W. The mammalian pyruvate dehydrogenase complex: Structure and regulation. in *Reviews of Physiology, Biochemistry and Pharmacology* 123–170 (Springer Berlin Heidelberg, 1983).

4. Korotchkina, L. G. & Patel, M. S. Mutagenesis studies of the phosphorylation sites of recombinant human pyruvate dehydrogenase. Site-specific regulation. *Journal of Biological Chemistry* **270**, 14297–14304 (1995).

5. Jeoung, N. H. Pyruvate dehydrogenase kinases: Therapeutic targets for diabetes and cancers. *Diabetes Metab. J.* **39**, 188–197 (2015).

6. P. B. Garland, E. A. Newsholme, and P. J. R. Regulation of Glucose Uptake by Muscle. *Biochem. J* **93**, 665–678 (1964).

7. Kolobova, E., Tuganova, a, Boulatnikov, I. & Popov, K. M. Regulation of pyruvate dehydrogenase activity through phosphorylation at multiple sites. *Biochem. J.* **358**, 69–77 (2001).

8. Bowker-Kinley, M. M., Davis, W. I., Wu, P., Harris, R. A. & Popov, K. M. Evidence for existence of tissue-specific regulation of the mammalian pyruvate dehydrogenase complex. *Biochem. J* **329**, 191–196 (1998).

9. T. E. Roche and Y. Hiromasa. Pdks regulation 2007. *Cell. Mol. Life Sci* **64**, 830–49 (2007).

10. Sugden, M. C. & Holness, M. J. Mechanisms underlying regulation of the expression and activities of the mammalian pyruvate dehydrogenase kinases. (2006). doi:10.1080/13813450600935263

11. Jeong, J. Y., Jeoung, N. H., Park, K.-G. & Lee, I.-K. Transcriptional Regulation of Pyruvate Dehydrogenase Kinase. *Diabetes Metab J* **36**, 328–335 (2012).

12. Semenza, G. L. oxygen regulation semenza 2009. *PHYSIOLOGY* **24**, 97–106 (2009).

13. Aragones, J., Fraisl, P., Baes, M. & Carmeliet, P. Oxygen Sensors at the Crossroad of Metabolism. *Cell Metabolism* (2009). doi:10.1016/j.cmet.2008.10.001

14. Papandreou, I., Cairns, R. A., Fontana, L., Lim, A. L. & Denko, N. C. HIF-1 mediates adaptation to hypoxia by actively downregulating mitochondrial oxygen consumption. *Cell Metab.* **3**, 187–197 (2006).

15. Kim, J. W., Tchernyshyov, I., Semenza, G. L. & Dang, C. V. HIF-1-mediated expression of pyruvate dehydrogenase kinase: A metabolic switch required for cellular adaptation to hypoxia. *Cell Metab.* (2006). doi:10.1016/j.cmet.2006.02.002

16. Kluza, J. *et al.* Inactivation of the HIF-1??/PDK3 signaling axis drives melanoma toward mitochondrial oxidative metabolism and potentiates the therapeutic activity of pro-oxidants. *Cancer Res.* (2012). doi:10.1158/0008-5472.CAN-12-0979

17. Lu, C. W., Lin, S. C., Chen, K. F., Lai, Y. Y. & Tsai, S. J. Induction of pyruvate dehydrogenase kinase-3 by hypoxia-inducible factor-1 promotes metabolic switch and drug resistance. *J. Biol. Chem.* **283**, 28106–28114 (2008).

18. Prigione, A. *et al.* HIF1?? modulates cell fate reprogramming through early glycolytic shift and upregulation of PDK1-3 and PKM2. *Stem Cells* (2014). doi:10.1002/stem.1552

19. Tennessen, J. M. *et al.* Coordinated Metabolic Transitions During Drosophila Embryogenesis and the Onset of Aerobic Glycolysis. doi:10.1534/g3.114.010652

20. Saunier, E., Benelli, C. & Bortoli, S. The pyruvate dehydrogenase complex in cancer: An old metabolic gatekeeper regulated by new pathways and pharmacological agents. *International Journal of Cancer* (2016). doi:10.1002/ijc.29564

21. Simon, M. C. & Keith, B. The role of oxygen availability in embryonic development and stem cell function. *Nat Rev Mol Cell Biol* **9**, 285–296 (2008).

22. Koh, M. Y. & Powis, G. Passing the baton: The HIF switch. *Trends Biochem. Sci.* **37**, 364–372 (2012).

23. Dunwoodie, S. L. The Role of Hypoxia in Development of the Mammalian Embryo. *Developmental Cell* (2009). doi:10.1016/j.devcel.2009.11.008

24. Amarilio, R. *et al.* HIF1alpha regulation of Sox9 is necessary to maintain differentiation of hypoxic prechondrogenic cells during early skeletogenesis. *Development* **134**, 3917–28 (2007).

25. Provot, S. *et al.* Hif-1?? regulates differentiation of limb bud mesenchyme and joint development. *J. Cell Biol.* (2007). doi:10.1083/jcb.200612023

26. Schipani, E. *et al.* Hypoxia in cartilage: HIF-1?? is essential for chondrocyte growth arrest and survival. *Genes Dev.* **15**, 2865–2876 (2001).

27. Hallmann R, Feinberg RN, Latker CH, Sasse J, R. W. Regression of blood vessels precedes cartilage differentiation during chick limb development. *Differentiation* **34**, 98–105 (1987).

28. Maes, C. *et al.* VEGF-independent cell-autonomous functions of HIF-1?? regulating oxygen consumption in fetal cartilage are critical for chondrocyte survival. *J. Bone Miner. Res.* **27**, 596–609 (2012).

29. Bentovim, L., Amarilio, R. & Zelzer, E. HIF1 is a central regulator of collagen hydroxylation and secretion under hypoxia during bone development. *Development* **139**, 4473–4483 (2012).

30. Vandenboom, R. *et al.* compensation PDH kinase 2 knockout mice: effect of PDH kinase 1 PDH activation during in vitro muscle contractions in PDH activation during in vitro muscle contractions in PDH kinase 2 knockout mice: effect of PDH kinase 1 compensation. *Am J Physiol Regul Integr Comp Physiol Am. J. Physiol. -Regulatory, Integr. Comp. Physiol. Weizmann Inst Sci* (2011). doi:10.1152/ajpregu.00498.2010

31. Ho Jeoung, N. *et al.* Role of pyruvate dehydrogenase kinase isoenzyme 4 (PDHK4) in glucose homoeostasis during starvation. *Biochem. J* **397**, 417–425 (2006).

32. Nam Ho Jeoung, Yasmeen Rahim,Pengfei Wu,W. N. Paul Lee, and R. A. & Harris. Fasting

induces ketoacidosis and hypothermia in PDHK2/ PDHK4-double-knockout mice. **443**, 829–839 (2012).

33. Semba, H. *et al.* HIF-1α-PDK1 axis-induced active glycolysis plays an essential role in macrophage migratory capacity. *Nat. Commun.* **7**, 1–10 (2016).

34. Prigione, A. *et al.* HIF1?? modulates cell fate reprogramming through early glycolytic shift and upregulation of PDK1-3 and PKM2. *Stem Cells* **32**, 364–376 (2014).

35. Provot, S. & Schipani, E. Molecular mechanisms of endochondral bone development. *Biochem. Biophys. Res. Commun.* **328**, 658–665 (2005).

36. Laffel, L. Ketone Bodies : a Review of Physiology , Pathophysiology and Application of Monitoring to Diabetes. 412–426 (1999).

37. Crabb DW, H. R. Mechanism responsible for the hypoglycemic actions of dichloroacetate and 2-chloropropionate. *Arch. Biochem. Biophys.* **198**, 145–152 (1979).

38. Paten, B., Herrero, J., Beal, K., Fitzgerald, S. & Birney, E. Enredo and Pecan : Genome-wide mammalian consistency-based multiple alignment with paralogs. 1814–1828 (2008). doi:10.1101/gr.076554.108.

39. Stelzer, G. *et al.* The GeneCards Suite : From Gene Data Mining to Disease Genome Sequence Analyses. 1–33 (2016). doi:10.1002/cpbi.5

40. Broquist, H. Amino Acid Metabolism. *Annu. Rev. Biochem.* **35**, 231–247 (1966).

41. Stelzer G, Inger A, Olender T, Iny-Stein T, Dalah I, Harel A, Safran M, L. D. GeneDecks: paralog hunting and gene-set distillation with GeneCards annotation. *Omi. A J. Integr. Biol.* **13**, (2009).

42. Szklarczyk, D. *et al.* The STRING database in 2017: Quality-controlled protein-protein association networks, made broadly accessible. *Nucleic Acids Res.* **45**, D362–D368 (2017).

43. Joshi MA, Jeoung NH, Obayashi M, Hattab EM, Brocken EG, Liechty EA, Kubek MJ, Vattem KM, Wek RC, H. R. Impaired growth and neurological abnormalities in branched-chain α -keto acid dehydrogenase kinase-deficient mice. *Biochem. J* **162**, 153–162 (2006).

44. Logan, M. *et al.* Expression of Cre Recombinase in the developing mouse limb bud driven by a Prxl enhancer. *Genesis* (2002). doi:10.1002/gene.10092

45. Stacpoole, P. W. The Pharmacology of Dichloroacetate. *Metabolism* **38**, 1124–1144 (1989).

46. Zhang, S., Zeng, X., Ren, M., Mao, X. & Qiao, S. Novel metabolic and physiological functions of branched chain amino acids: A review. *J. Anim. Sci. Biotechnol.* **8**, 4–15 (2017).

47. Zhou, M., Lu, G., Gao, C., Wang, Y. & Sun, H. Tissue-specific and Nutrient Regulation of the Branched-chain ␣ -Keto Acid Dehydrogenase Phosphatase , Protein Phosphatase 2Cm (PP2Cm) * □. **287**, 23397–23406 (2012).

48. Nishitani, S. *et al.* Branched-chain amino acids improve glucose metabolism in rats with liver cirrhosis. 1292–1300 (2019). doi:10.1152/ajpgi.00510.2003.

49. Shao, D. *et al.* branched-chain amino acid degradation. *Nat. Commun.* (2018). doi:10.1038/s41467-018-05362-7

50. Oppenheim, R. D. *et al.* BCKDH: The Missing Link in Apicomplexan Mitochondrial Metabolism Is Required for Full Virulence of Toxoplasma gondii and Plasmodium berghei. *PLoS Pathog.* **10**, (2014).

51. Wynn, R. M., Chuang, J. L., Cote, C. D. & Chuang, D. T. Tetrameric Assembly and Conservation in the ATP-binding Domain of Rat Branched-chain ␣ -Ketoacid Dehydrogenase Kinase *. **275**, 30512–30519 (2000).

52. Gudi, R. *et al.* Diversity of the Pyruvate Dehydrogenase Kinase Gene Family in Humans. *Cell Biol. Metab.* **270**, 28989–28994 (1995).

53. K M Popov, N Y Kedishvili, Y Zhao, Y Shimomura, D. W. C. and R. A. H. Primary Structure of Pyruvate Dehydrogenase Kinase Establishes a New Family of Eukaryotic Protein Kinases *. *J. Biol. Chem.* **268**, 26602–26606 (1993).

54. Ferriero, R. *et al.* Phenylbutyrate Therapy for Pyruvate Dehydrogenase Complex Deficiency Phenylbutyrate Therapy for Pyruvate Dehydrogenase Complex Deficiency and Lactic Acidosis. **175**, (2013).

55. Ciszak, E. M., Korotchkina, L. G., Dominiak, P. M., Sidhu, S. & Patel, M. S. Structural Basis for Flip-Flop Action of Thiamin Pyrophosphate- dependent Enzymes Revealed by Human Pyruvate Dehydrogenase *. **278**, 21240–21246 (2003).

56. Kidney, B. *et al.* Sites of Phosphorylation on Pyruvate Dehydrogenase. 2364–2370 (1978). doi:10.1021/bi00605a017

57. Sugden, M. C. & Holness, M. J. complex by PDKs oxidation at the level of the pyruvate dehydrogenase Recent advances in mechanisms regulating glucose Recent advances in mechanisms regulating glucose oxidation at the level of the pyruvate dehydrogenase complex by PDKs. *Am J Physiol Endocrinol Metab Am. J. Physiol. -Endocrinology Metab. by guest* **284**, 855–862 (2003).

58. Korotchkina, L. G. Site Specificity of Four Pyruvate Dehydrogenase Kinase Isoenzymes toward the Three Phosphorylation Sites of Human Pyruvate Dehydrogenase *. **276**, 37223–37229 (2001).

59. Sale, G. J. & Randle, P. J. Role of individual phosphorylation sites in inactivation of pyruvate dehydrogenase complex in rat heart mitochondria. **1**, 99–108 (1982).

60. Semenza, G. L. Hypoxia-inducible factor 1 : oxygen homeostasis and disease pathophysiology. *TRENDS Mol. Med.* **7**, 345–350 (2001).

61. Kim, J. W., Tchernyshyov, I., Semenza, G. L. & Dang, C. V. HIF-1-mediated expression of pyruvate dehydrogenase kinase: A metabolic switch required for cellular adaptation to hypoxia. *Cell Metab.* **3**, 177–185 (2006).

62. Weissgerber, T. L. & Wolfe, L. A. Physiological adaptation in early human pregnancy : adaptation to balance maternal – fetal demands. **11**, 1–11 (2006).

63. Pettitt, S. J. *et al.* Europe PMC Funders Group Agouti C57BL / 6N embryonic stem cells for mouse genetic resources. **6**, 493–495 (2013).

64. Lallemand, Y., Luria, V., Haffner-Krausz, R. & Lonai, P. Maternally expressed PGK-Cre transgene as a tool for early and uniform activation of the Cre site-specific recombinase. *Transgenic Res.* (1998). doi:10.1023/A:1008868325009

65. Hsu, P. D. *et al.* DNA targeting specificity of RNA-guided Cas9 nucleases. **31**, (2013).

66. Doench, J. G. *et al.* Rational design of highly active sgRNAs for CRISPR-Cas9 – mediated gene inactivation. *Nat. Biotechnol.* **32**, (2014).

67. Doench, J. G. *et al.* Optimized sgRNA design to maximize activity and minimize off-target effects of CRISPR-Cas9. *Nat. Biotechnol.* **34**, 184–191 (2016).

68. Xu, H. *et al.* Sequence determinants of improved CRISPR sgRNA design. 1147–1157 (2015). doi:10.1101/gr.191452.115.10

69. Chari, R., Moosburner, M. & Church, G. M. Unraveling CRISPR-Cas9 genome engineering parameters via a library- on-library approach. **12**, (2015).

70. Jaenisch, R. *et al.* One-step generation of mice carrying mutations in multiple genes by CRISPR/Cas-mediated genome engineering. *Cell* **153**, 910–918 (2013).

71. Eshkar-oren, I. *et al.* The forming limb skeleton serves as a signaling center for limb vasculature patterning via regulation of Vegf. **1272**, 1263–1272 (2009).

72. Mcleod, M. J. Differential Staining of Cartilage and Bone in Whole Mouse Fetuses by Alcian Blue and Alizarin Red S. **301**, 299–301 (1980).

73. Zheng, L. *et al.* Fumarate induces redox-dependent senescence by modifying glutathione metabolism. *Nat. Commun.* **6**, 1–12 (2015).

74. Caspi, R. *et al.* The MetaCyc database of metabolic pathways and enzymes. *Nucleic Acids Res.* **46**, D633–D639 (2018).